ACS APPLIED MATERIALS & INTERFACES

www.acsami.org

Research Article

Hierarchical Porous Carbon Arising from Metal–Organic Framework-Encapsulated Bacteria and Its Energy Storage Potential

Shaobo Li, Xiaoshuang Zhou, Zhuo Chen, Fabian C. Herbert, Rangana Jayawickramage, Samitha D. Panangala, Michael A. Luzuriaga, Sampath B. Alahakoon, Shashini D. Diwakara, Xin Meng, Ling Fei, John Ferraris, Ronald A. Smaldone, and Jeremiah J. Gassensmith*

Cite This: https://dx.doi.org/10.1021/acsami.9b15667

Read Online

ACCESS | Metrics & More | Article Recommendations | Supporting Information

ABSTRACT: Hierarchical porous carbons (HPCs) hold great promise in energy-related applications owing to their excellent chemical stability and well-developed porous structures. Attention has been drawn toward developing new synthetic strategies and precursor materials that permit greater control over composition, size, morphology, and pore structure. There is a growing trend of employing metal–organic frameworks (MOFs) as HPC precursors as their highly customizable characteristics favor new HPC syntheses. In this article, we report a biomimetically grown bacterial-templated MOF synthesis where the bacteria not only facilitate the formation of MOF nanocrystals but also provide morphology and porosity control. The resultant HPCs show improved electrochemical capacity behavior compared to pristine MOF-derived HPCs. Considering the broad availability of bacteria and ease of their production, in addition to significantly improved MOF growth efficiency on bacterial templates, we believe that the bacterial-templated MOF is a promising strategy to produce a new generation of HPCs.

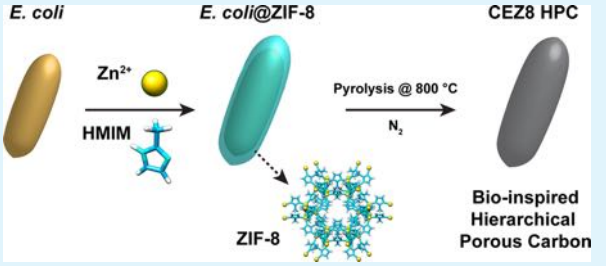

KEYWORDS: *hierarchical porous carbon, metal–organic frameworks, biomimetic mineralization, bacteria, carbonization, supercapacitor*

INTRODUCTION

Hierarchical porous carbons (HPC) are a class of materials that are fabricated to obtain high surface areas, multiscale porosities, heteroatom doping, excellent conductivity, and outstanding stability. These characteristics are highly sought after in adsorbents, catalysis, and energy conversion and storage.[1−6] Conventional fabrication of HPCs relies on utilizing synthetic inorganic/organic templates or chemical activation, which generally requires multiple steps beginning with template syntheses, followed by precursor infiltration, carbonization, and template removal to generate the desired heterogenous porosity.[1−3,7] These tedious synthetic processes inevitably increase the complexity and cost of HPC preparation, thus hindering the eventual mass production and commercialization of such promising materials. Over the previous two decades, metal–organic frameworks (MOFs) have become a popular architecture for advanced materials owing to their highly customizable pore structure, composition, and straightforward synthetic strategies.[8−12] MOFs are also recognized as promising precursors for porous carbons. Because of their characteristic porous nature and high carbon content, MOFs enable facile conversion to porous carbons possessing high surface area with an inner-connected porous architecture.[13−18] For example, Xu et al. demonstrated[19] excellent electrochemical performance with porous carbon that was derived from pyrolyzing furfuryl alcohol-filled MOF-5. Since then, more MOF-derived carbons, metal oxides, metal sulfides, and hybrid materials have been developed, showing the versatility of MOF-based precursors.[17,18,20]

In recent years, templated MOF synthesis with biologically derived substrates has begun producing an ever-growing array of bio-MOF composites featuring morphology and size that are dictated, in part, by the underlying biological material used. In addition to potential benefits such as environmental friendliness, low cost, and high efficiency,[21−30] the available biomass to template MOF syntheses is extraordinary—viruses[25,26,31] and yeast[23,24,30] have already been shown to be outstanding templates to produce core–shell systems—and researchers have only begun to explore the potential uses of biomass as homogenous and low-cost templates for new MOF architectures. Bacteria's high reproduction rate and natural abundance make them an ideal source of cheap precursor materials—indeed our body contains at least three times more bacterial cells than human cells! In addition to its ubiquity, the diversity of shapes and assemblies (Scheme 1) can provide multiple morphological templates for biomimetic MOF syntheses.

Received: September 4, 2019
Accepted: February 13, 2020
Published: February 13, 2020

Scheme 1. Schematic Illustration of Various Bacterial Shapes and Assemblies

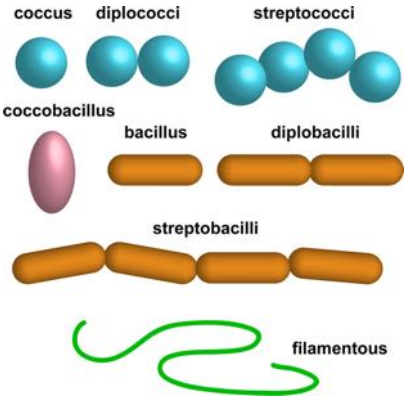

Herein, we report a bio-inspired preparation of MOF-derived HPCs driven by a robust bacterial template, as shown in Scheme 2. A nonpathogenic nontoxic laboratory strain of

Scheme 2. Schematic Illustration of Synthetic Processes of CEZ8 HPC (Top) and CZ8 HPC (Bottom), which Used the *E. coli*@ZIF-8 Composite and Pristine ZIF-8 as Precursors, Respectively

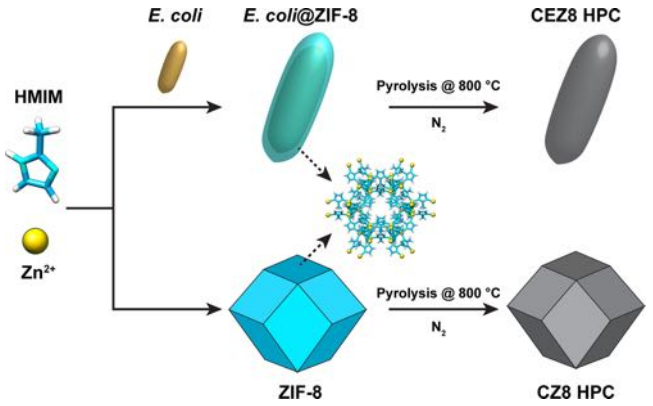

Escherichia coli was employed to construct a thin crystalline shell of zeolitic imidazolate framework-8 (ZIF-8), a widely used MOF carbonization precursor owing to its extraordinary surface area and stability.[10] Interestingly, the resultant *E. coli*@ZIF-8 (EZ8) composite possesses not only well-defined micropores but also mesopores and macropores that can be attributed to the disturbed crystal growth on the cell membrane. As anticipated, this pore hierarchy can be retained after carbonization of EZ8. The as-obtained carbonized EZ8 (CEZ8) is considerably more mesoporous compared to its parent material. The electrochemical characteristics of CEZ8 were tested in a standard three-electrode system, and we observed superior specific capacity compared to carbonized pristine ZIF-8 (denoted as CZ8).

RESULTS & DISCUSSION

Preparation of *E. coli*@ZIF-8 (EZ8). The hierarchical porous structure and unique rod-like morphology of CEZ8 HPC is attributed to growing a thin polycrystalline ZIF-8 shell on *E. coli*. In the last few years, our group has investigated ZIF-8 growth on biological substrates to produce templated architectures. By utilizing tobacco mosaic virus (TMV) as a model template, we revealed that surface interactions with the protein bio-nanoparticles combined with the synthetic conditions of precursor solutions play critical roles in ZIF-8 growth. In particular, we found that the nanometer-thick core–shell ZIF-8 structures are formed with virus particles only when the precursor solutions are selected such that they initially produce the kinetic amorphous metal-coordination products first rather than monolithic ZIF-8 crystals. These kinetic products form from a relatively low concentration (400 mM) of ligand (2-methylimidazole, HMIM) solution and a low ligand to metal molar ratio (L/M ratio, 20:1). Ultimately, these kinetic products ripen to polycrystalline ZIF-8 shells. We thought that bacterial cells, which contain lipopolysaccharide-rich bilayers (e.g., Gram-negative *E. coli*) or exposed peptidoglycan cell walls (e.g., Gram-positive *Enterococcus faecium*), can induce ZIF-8 nucleation and crystal growth in a similar manner. To our surprise, the optimal ZIF-8 growth conditions on *E. coli* were found to be opposite to what we had discovered on TMV. This new approach differs from previous efforts to grow ZIF-8 on bionanoparticle substrates (enzyme[21,29] and virus[25,26]) in a number of important ways. In particular, a much higher precursor concentration (1600 mM) and L/M ratio (80:1) must be used to promote the crystal growth on the surface of bacteria. Curiously, our synthesis yields a ZIF-8 shell that is more homogeneous and thinner (Figure 1a,c) than the examples that were found on

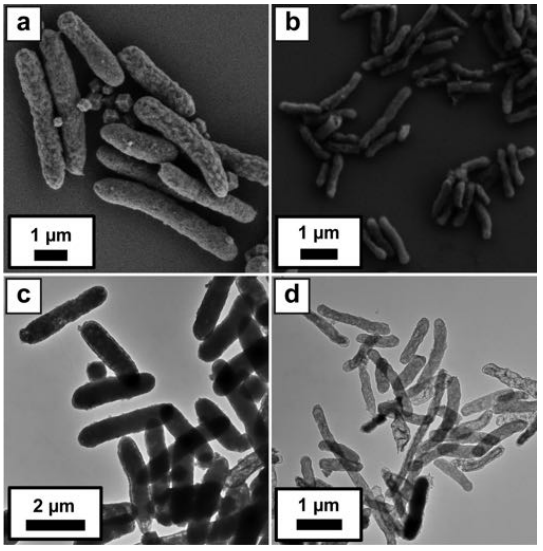

Figure 1. Scanning electron microscopy micrographs of (a) uncarbonized EZ8 and (b) carbonized CEZ8; TEM micrographs of (c) EZ8 and (d) CEZ8.

yeast cells.[30] We attribute it to the high ligand concentration and high L/M ratio, which work together to boost the formation of ZIF-8 nanocrystalites.[25] In a typical synthesis, purified *E. coli* (1 mg) was mixed with an aliquot of HMIM aqueous solution (1600 mM) followed by an aliquot of zinc acetate aqueous solution (20 mM). The mixture was shaken for 20 s and left on the benchtop for 30 min. The as-formed EZ8 was collected by centrifugation at 4300*g* and then washed twice with ultrapure water. As shown in Figure 1, EZ8 retains the rod-like morphology of bacteria (Figure 1a), and the light/dark contrast in the transmission electron microscopy (TEM) micrograph clearly illustrates the core–shell structure (Figure 1c). High-magnification TEM micrographs (Figure S1a)

https://dx.doi.org/10.1021/acsami.9b15667
ACS Appl. Mater. Interfaces XXXX, XXX, XXX–XXX

illustrate clearly that the shells are composed of closely packed nanocrystals. To analyze crystallinity and phase purity, EZ8 dry powder was analyzed by powder X-ray diffraction (PXRD) (Figure 2a), and the result shows the pure sodalite crystalline

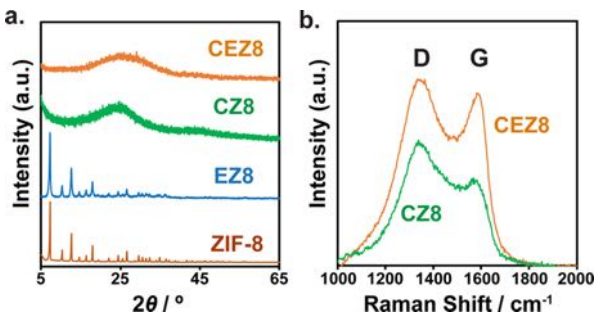

Figure 2. (a) PXRD patterns of the as-prepared ZIF-8, *E. coli*@ZIF-8 (EZ8), carbonized ZIF-8 (CZ8), and carbonized *E. coli*@ZIF-8 (CEZ8); (b) Raman spectra of CZ8 and CEZ8.

phase of ZIF-8. To demonstrate the generalizability of this approach, we also encapsulated *E. faecium* bacteria, a spherical Gram-positive bacterium found in everyone's colon, and we observed similar coatings of sodalite ZIF-8 (Figure S2).

The nitrogen sorption isotherm was collected at 77 K to obtain the specific surface area and pore size distribution of EZ8 and pristine ZIF-8, as shown in Figure S4. The as-prepared pristine ZIF-8 possesses a typical type I isotherm with a sharp uptake at low relative pressure (<0.03), indicating the presence of micropores (Figure S4a); however, in addition to the similar microporous pattern, EZ8 also contains a H3 hysteresis loop at a relative pressure of 0.45−1.0, which typically indicates capillary condensation of the adsorbate (N_2) in mesopores. The calculated Brunauer−Emmett−Teller surface areas of ZIF-8 and EZ8 are 1842 and 1209 m^2/g, respectively (Table S1). As shown in Figure S4b, the pore distribution analysis uncovered two intense peaks at 1.1 nm in both ZIF-8 and EZ8, while a lower hump around 10 and 63 nm indicates hierarchical pore characteristics in EZ8. We attributed the presence of mesopores to crystalline defects arising from the drastic crystallization on the surface of bacterial cell membranes, and we anticipated that the mesoporous characteristics of the shell can be further developed during carbonization.

Preparation of Carbonized *E. coli*@ZIF-8 (CEZ8). Carbonization was carried out by temperature-programmed pyrolysis for both EZ8 and ZIF-8. Materials were dried at 120 °C under dynamic vacuum overnight prior to pyrolysis in a tube furnace with a nitrogen atmosphere. The temperature was raised with a 5 °C/min ramp to 350 °C and kept at 350 °C for 2 h. We utilized this process to ablate bacterial matter without impacting the stability of the ZIF-8 shells, owing to the large thermal stability differences between *E. coli* and ZIF-8, as revealed by thermogravimetric analysis (Figure S5). Following bacterial template ablation, the furnace was thermally ramped to 800 °C with the same rate and kept at 800 °C for 4 h. The carbonized products appeared as black powder and were washed with 2 M HCl and 10% HF to remove residual zinc in the products. The carbonized *E. coli*@ZIF-8, denoted as CEZ8, retained rod-like morphology of EZ8, although a certain level of shrinkage (Figure 1b) was observed. TEM (Figure 1d) revealed an enhanced transparency at the inner part of CEZ8 rods. The hollowness of these rod-like structures indicates the ablation of the unstable proteinaceous content. At high magnification in TEM (Figure S1c), we observed a large number of high contrast dots on the surface of the CEZ8 rods, which can be attributed to defects or nanopores that were generated during carbonization. These observations are consistent with the hysteresis loop in the N_2 sorption isotherm (Figure 3a) and pore analysis that shows peaks in the

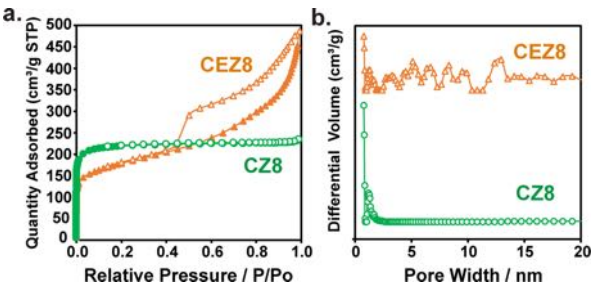

Figure 3. (a) N_2 sorption analysis of CZ8 and CEZ8; (b) porosity distribution of CZ8 and CEZ8.

mesoporous range (Figure 3b). Furthermore, we noticed that the pore volume of meso- and macropores of CEZ8 was much higher than that of EZ8. We suspect that the development of these large pores results from the different phase change processes at the bacteria−ZIF-8 interface during pyrolysis. The microstructure of carbonized materials was characterized by PXRD (Figure 2a). Both CEZ8 and CZ8 contain only a broad peak at about 25°, which can be attributed to the (002) peak of graphitic carbon. The content of graphitic carbon in comparison to amorphous carbon was revealed by Raman spectroscopy (Figure 2b), and the I_D/I_G values were calculated as 1.07 for CEZ8 and 1.45 for CZ8, indicating that the *E. coli*@ZIF-8 composite yields a higher content of graphitic carbon than pristine ZIF-8. The chemical composition was characterized by X-ray photoelectron spectroscopy (XPS), as shown in Figure S7. Both CZ8 and CEZ8 have a high content of nitrogen. The deconvoluted N 1s peak (Figure S8) revealed pyridinic, pyrrolic, and graphitic N, indicating heteroatom doping of carbon. It is also worth noting that CEZ8 has higher doped O species than CZ8 (Figure S7c).

Electrochemical Characterization. Owing to the high content of graphitic carbon and well-developed hierarchical porosity, we were encouraged to investigate the electrochemical properties of CEZ8 in energy storage. A standard three-electrode cell with Ag/AgCl and platinum mesh as the reference electrode and counter electrode, respectively, in 6 M KOH aqueous solution as the electrolyte was used to evaluate the capacitive behavior of CEZ8, CZ8, and carbonized *E. coli* (C-*E. coli*). Cyclic voltammograms (Figures 4a,b, and S9a) were recorded in the voltage window from −0.6 to 0.2 V, and specific capacitance was calculated accordingly, as illustrated in Figure 4c and Table S2. We found that CZ8 contained the typical rectangular cyclic voltammogram of electrostatic double-layer capacitors, whereas the distorted cyclic voltammogram shapes of CEZ8 and C-*E. coli* appear to show pseudocapacitance from the residual carbonized bacterial substrate.[32] This also agrees with the relatively higher oxygen doping in CEZ8 from the XPS result (Figure S7c). The highest specific capacitances of CEZ8, CZ8, and C-*E. coli* were found to be 163, 87, and 17 F/g, respectively, at a scan rate of 5 mV/s, indicating a superior capacitive behavior of CEZ8. We note that CEZ8 actually contains a lower specific surface area

https://dx.doi.org/10.1021/acsami.9b15667
ACS Appl. Mater. Interfaces XXXX, XXX, XXX−XXX

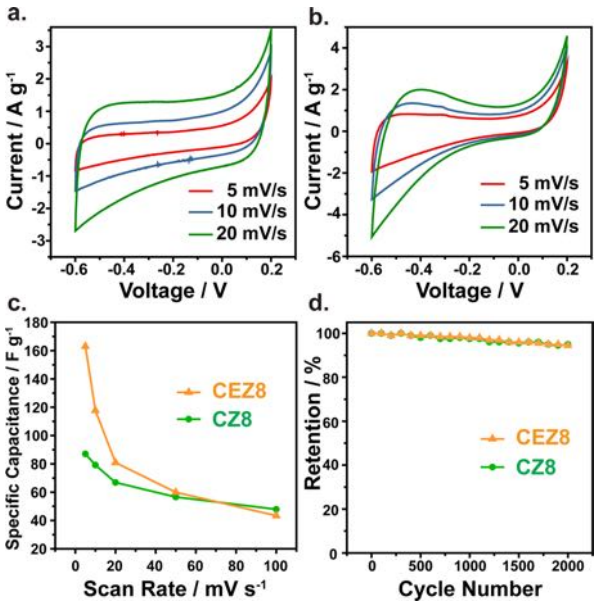

Figure 4. Cyclic voltammograms at different sweep rates of (a) CZ8 and (b) CEZ8; (c) specific capacitance as a function of scan rate for CZ8 and CEZ8; and (d) cycling stability of CZ8 and CEZ8.

compared to CZ8 (645 m^2/g vs 841 m^2/g) because the carbonized bacteria in CEZ8 do not contribute to the porosity (Figure S9c,d).[32] We therefore attribute the superior performance of CEZ8 to the synergetic effect of hierarchical porosity and its higher content of graphitic carbon formed at the bacteria–ZIF-8 interface. This is reflected in the fast fadeaway of capacity when CEZ8 was tested under higher scan rates, in comparison to CZ8 (Figure 4c). As Xu et al.[33] have shown, the presence of mesopores does not guarantee excellent rate performance if these pores are not well interconnected. The thermal degradation of bacteria inside ZIF-8 produces random mesopores at the bacteria–ZIF-8 interface, which are likely not completely interconnected. Thus, we observe low ion transport efficiency at higher scan rates but very good transport at low scan rates. Nevertheless, both CEZ8 and CZ8 show excellent cyclability as they demonstrate 94.5 and 95% retention after 2000 cycles (Figure 4d), which we ascribe to their robust structural stability.

CONCLUSIONS

In this work, we demonstrated a new strategy to prepare HPCs via straightforward and convenient biomimetic mineralization of ZIF-8 using nonpathogenic and nontoxic bacterial cells. We found that bacterial cell surfaces efficiently nucleate the rapid crystallization of ZIF-8, which produces a crystalline shell that can be carbonized into a material possessing a hierarchy of porosities. The bacterial template is thermally ablated during carbonization and contributes to a higher level of graphitization of the ZIF-8 shell during pyrolysis. The as-prepared CEZ8 possesses superior capacitive performance to carbonized pristine ZIF-8 owing to the incorporation of well-developed hierarchical porosity, good conductivity, and pseudocapacitance at the bacteria–ZIF-8 interface. Although carbonized MOFs with a higher capacity have been reported[33−36] elsewhere, we believe that further optimization of CEZ8 in terms of microporosity, pore interconnection, and surface area can lead to competitive capacitive performance. We further believe that the size and morphological diversity of bacteria and their high reproduction rate means that they hold great promise in templating and fabricating HPC materials.

EXPERIMENTAL SECTION

All material fabrication procedures, characterization methods, and supplementary data are summarized in the Supporting Information.

ASSOCIATED CONTENT

Supporting Information

The Supporting Information is available free of charge at https://pubs.acs.org/doi/10.1021/acsami.9b15667.

Experimental procedure, characterization techniques, and additional characterization results (PDF)

AUTHOR INFORMATION

Corresponding Author

Jeremiah J. Gassensmith − *Department of Chemistry and Biochemistry and Department of Biomedical Engineering, The University of Texas at Dallas, Richardson, Texas 75080, United States;* orcid.org/0000-0001-6400-8106; Phone: (972) 883-3596; Email: gassensmith@utdallas.edu, www.gassensmithlab.com

Authors

Shaobo Li − *Department of Chemistry and Biochemistry, The University of Texas at Dallas, Richardson, Texas 75080, United States;* orcid.org/0000-0002-4178-0897

Xiaoshuang Zhou − *Jiangsu Collaborative Innovation Center of Photovoltaic Science and Engineering, Changzhou University, Changzhou 213164, China*

Zhuo Chen − *Department of Chemistry and Biochemistry, The University of Texas at Dallas, Richardson, Texas 75080, United States;* orcid.org/0000-0001-7775-7579

Fabian C. Herbert − *Department of Chemistry and Biochemistry, The University of Texas at Dallas, Richardson, Texas 75080, United States*

Rangana Jayawickramage − *Department of Chemistry and Biochemistry, The University of Texas at Dallas, Richardson, Texas 75080, United States*

Samitha D. Panangala − *Department of Chemistry and Biochemistry, The University of Texas at Dallas, Richardson, Texas 75080, United States;* orcid.org/0000-0002-1396-2132

Michael A. Luzuriaga − *Department of Chemistry and Biochemistry, The University of Texas at Dallas, Richardson, Texas 75080, United States;* orcid.org/0000-0001-6128-8800

Sampath B. Alahakoon − *Department of Chemistry and Biochemistry, The University of Texas at Dallas, Richardson, Texas 75080, United States*

Shashini D. Diwakara − *Department of Chemistry and Biochemistry, The University of Texas at Dallas, Richardson, Texas 75080, United States*

Xin Meng − *Department of Electrical Engineering, The University of Texas at Dallas, Richardson, Texas 75080, United States;* orcid.org/0000-0003-0933-6419

Ling Fei − *Department of Chemical Engineering, University of Louisiana at Lafayette, Lafayette, Louisiana 70504, United States;* orcid.org/0000-0002-0954-5168

John Ferraris − *Department of Chemistry and Biochemistry, The University of Texas at Dallas, Richardson, Texas 75080, United States;* orcid.org/0000-0002-3225-0093

https://dx.doi.org/10.1021/acsami.9b15667
ACS Appl. Mater. Interfaces XXXX, XXX, XXX−XXX

Ronald A. Smaldone − *Department of Chemistry and Biochemistry, The University of Texas at Dallas, Richardson, Texas 75080, United States;* orcid.org/0000-0003-4560-7079

Complete contact information is available at: https://pubs.acs.org/10.1021/acsami.9b15667

Author Contributions

S.L. planned and conducted the synthesis and characterization of CEZ8. X.Z. conducted CV measurements for carbonized ZIF samples and analyzed the electrochemical results. Z.C. and F.C.H. conducted bacterial strain preparation, isolation, and encapsulation. R.J. conducted pyrolysis of all samples and Raman characterization. S.B.A. and S.L. performed nitrogen sorption experiments and BET analysis. X.M. conducted XPS characterization. L.F. provided an electrochemical workstation and CV instrumentation for carbonized *E. coli* at the University of Louisiana at Lafayette. M.A.L. took SEM images of *E. coli*@ZIF-8 and *E. faecium* 733@ZIF-8. J.F. provided tube furnaces and a Raman spectrometer and supervised R.J. R.A.S. provided porosity instrumentation and supervised S.B.A. J.J.G. conceived the project with S.L. S.L. and J.J.G. composed the manuscript. All authors read and approved the final manuscript.

Funding

J.J.G. wishes to thank the Robert A. Welch Foundation [AT-1989-20190330] for funding this research and the National Science Foundation [CAREER DMR-1654405] for funding the integration of his entire scholarly and educational activities.

Notes

The authors declare no competing financial interest.

■ ACKNOWLEDGMENTS

E. faecium 773 was kindly supplied by the laboratory of Dr. Kelli Palmer, and *E. coli* DH5α was kindly provided by the laboratory of Dr. Sheena D'Arcy.

■ REFERENCES

(1) Lee, J.; Kim, J.; Hyeon, T. Recent Progress in the Synthesis of Porous Carbon Materials. *Adv. Mater.* **2006**, *18*, 2073−2094.
(2) Hu, Y.-S.; Adelhelm, P.; Smarsly, B. M.; Hore, S.; Antonietti, M.; Maier, J. Synthesis of Hierarchically Porous Carbon Monoliths with Highly Ordered Microstructure and Their Application in Rechargeable Lithium Batteries with High-Rate Capability. *Adv. Funct. Mater.* **2007**, *17*, 1873−1878.
(3) Roberts, A. D.; Li, X.; Zhang, H. Porous Carbon Spheres and Monoliths: Morphology Control, Pore Size Tuning and Their Applications as Li-ion Battery Anode Materials. *Chem. Soc. Rev.* **2014**, *43*, 4341−4356.
(4) Zhai, Y.; Dou, Y.; Zhao, D.; Fulvio, P. F.; Mayes, R. T.; Dai, S. Carbon Materials for Chemical Capacitive Energy Storage. *Adv. Mater.* **2011**, *23*, 4828−4850.
(5) Zhu, C.; Li, H.; Fu, S.; Du, D.; Lin, Y. Highly Efficient Nonprecious Metal Catalysts Towards Oxygen Reduction Reaction Based on Three-dimensional Porous Carbon Nanostructures. *Chem. Soc. Rev.* **2016**, *45*, 517−531.
(6) Wang, C.; Kaneti, Y. V.; Bando, Y.; Lin, J.; Liu, C.; Li, J.; Yamauchi, Y. Metal−organic Framework-derived One-Dimensional Porous or Hollow Carbon-based Nanofibers for Energy Storage and Conversion. *Mater. Horiz.* **2018**, *5*, 394−407.
(7) Liang, C.; Li, Z.; Dai, S. Mesoporous Carbon Materials: Synthesis and Modification. *Angew. Chem., Int. Ed.* **2008**, *47*, 3696−3717.
(8) Furukawa, H.; Cordova, K. E.; O'Keeffe, M.; Yaghi, O. M. The Chemistry and Applications of Metal-Organic Frameworks. *Science* **2013**, *341*, 1230444.
(9) Yaghi, O. M.; O'Keeffe, M.; Ockwig, N. W.; Chae, H. K.; Eddaoudi, M.; Kim, J. Reticular Synthesis and the Design of New Materials. *Nature* **2003**, *423*, 705.
(10) Park, K. S.; Ni, Z.; Cote, A. P.; Choi, J. Y.; Huang, R.; Uribe-Romo, F. J.; Chae, H. K.; O'Keeffe, M.; Yaghi, O. M. Exceptional Chemical and Thermal Stability of Zeolitic Imidazolate Frameworks. *Proc. Natl. Acad. Sci. U.S.A.* **2006**, *103*, 10186−10191.
(11) Bara, D.; Wilson, C.; Mörtel, M.; Khusniyarov, M. M.; Ling, S.; Slater, B.; Sproules, S.; Forgan, R. S. Kinetic Control of Interpenetration in Fe−Biphenyl-4,4′-dicarboxylate Metal−Organic Frameworks by Coordination and Oxidation Modulation. *J. Am. Chem. Soc.* **2019**, *141*, 8346−8357.
(12) Song, D.; Bae, J.; Ji, H.; Kim, M.-B.; Bae, Y.-S.; Park, K. S.; Moon, D.; Jeong, N. C. Coordinative Reduction of Metal Nodes Enhances the Hydrolytic Stability of a Paddlewheel Metal−Organic Framework. *J. Am. Chem. Soc.* **2019**, *141*, 7853−7864.
(13) Indra, A.; Song, T.; Paik, U. Metal Organic Framework Derived Materials: Progress and Prospects for the Energy Conversion and Storage. *Adv. Mater.* **2018**, *30*, 1705146.
(14) Zhu, B.; Xia, D.; Zou, R. Metal-organic Frameworks and Their Derivatives as Bifunctional Eectrocatalysts. *Coord. Chem. Rev.* **2018**, *376*, 430−448.
(15) Li, X.; Zheng, S.; Jin, L.; Li, Y.; Geng, P.; Xue, H.; Pang, H.; Xu, Q. Metal-Organic Framework-Derived Carbons for Battery Applications. *Adv. Energy Mater.* **2018**, *8*, 1800716.
(16) Zhang, H.; Liu, X.; Wu, Y.; Guan, C.; Cheetham, A. K.; Wang, J. MOF-derived Nanohybrids for Electrocatalysis and Energy Storage: Current Status and Perspectives. *Chem. Commun.* **2018**, *54*, 5268−5288.
(17) Xia, W.; Mahmood, A.; Zou, R.; Xu, Q. Metal−organic Frameworks and Their derived Nanostructures for Electrochemical Energy Storage and Conversion. *Energy Environ. Sci.* **2015**, *8*, 1837−1866.
(18) Salunkhe, R. R.; Kaneti, Y. V.; Kim, J.; Kim, J. H.; Yamauchi, Y. Nanoarchitectures for Metal−Organic Framework-Derived Nanoporous Carbons toward Supercapacitor Applications. *Acc. Chem. Res.* **2016**, *49*, 2796−2806.
(19) Liu, B.; Shioyama, H.; Akita, T.; Xu, Q. Metal-Organic Framework as a Template for Porous Carbon Synthesis. *J. Am. Chem. Soc.* **2008**, *130*, 5390−5391.
(20) Liang, Z.; Zhao, R.; Qiu, T.; Zou, R.; Xu, Q. Metal-organic Framework-derived Materials for Electrochemical Energy Applications. *EnergyChem* **2019**, *1*, 100001.
(21) Wu, X.; Yang, C.; Ge, J. Green Synthesis of Enzyme/Metal-organic Framework Composites with High Stability in Protein Denaturing Solvents. *Bioresour. Bioprocess.* **2017**, *4*, 24.
(22) Liang, W.; Ricco, R.; Maddigan, N. K.; Dickinson, R. P.; Xu, H.; Li, Q.; Sumby, C. J.; Bell, S. G.; Falcaro, P.; Doonan, C. J. Control of Structure Topology and Spatial Distribution of Biomacromolecules in Protein@ZIF-8 Biocomposites. *Chem. Mater.* **2018**, *30*, 1069−1077.
(23) Liang, K.; Richardson, J. J.; Doonan, C. J.; Mulet, X.; Ju, Y.; Cui, J.; Caruso, F.; Falcaro, P. An Enzyme-Coated Metal−Organic Framework Shell for Synthetically Adaptive Cell Survival. *Angew. Chem., Int. Ed.* **2017**, *56*, 8510−8515.
(24) Liang, K.; Richardson, J. J.; Cui, J.; Caruso, F.; Doonan, C. J.; Falcaro, P. Metal−Organic Framework Coatings as Cytoprotective Exoskeletons for Living Cells. *Adv. Mater.* **2016**, *28*, 7910−7914.
(25) Li, S.; Dharmarwardana, M.; Welch, R. P.; Benjamin, C. E.; Shamir, A. M.; Nielsen, S. O.; Gassensmith, J. J. Investigation of Controlled Growth of Metal−Organic Frameworks on Anisotropic Virus Particles. *ACS Appl. Mater. Interfaces* **2018**, *10*, 18161−18169.
(26) Li, S.; Dharmarwardana, M.; Welch, R. P.; Ren, Y.; Thompson, C. M.; Smaldone, R. A.; Gassensmith, J. J. Template-Directed Synthesis of Porous and Protective Core−Shell Bionanoparticles. *Angew. Chem., Int. Ed.* **2016**, *55*, 10691−10696.

(27) Riccò, R.; Liang, W.; Li, S.; Gassensmith, J. J.; Caruso, F.; Doonan, C.; Falcaro, P. Metal−Organic Frameworks for Cell and Virus Biology: A Perspective. *ACS Nano* **2018**, *12*, 13−23.
(28) Lyu, F.; Zhang, Y.; Zare, R. N.; Ge, J.; Liu, Z. One-Pot Synthesis of Protein-Embedded Metal−Organic Frameworks with Enhanced Biological Activities. *Nano Lett.* **2014**, *14*, 5761−5765.
(29) Liang, K.; Ricco, R.; Doherty, C. M.; Styles, M. J.; Bell, S.; Kirby, N.; Mudie, S.; Haylock, D.; Hill, A. J.; Doonan, C. J.; Falcaro, P. Biomimetic Mineralization of Metal-organic Frameworks as Protective Coatings for Biomacromolecules. *Nat. Commun.* **2015**, *6*, 7240.
(30) Li, W.; Zhang, Y.; Xu, Z.; Meng, Q.; Fan, Z.; Ye, S.; Zhang, G. Assembly of MOF Microcapsules with Size-Selective Permeability on Cell Walls. *Angew. Chem., Int. Ed.* **2015**, *55*, 955−959.
(31) Luzuriaga, M. A.; Welch, R. P.; Dharmarwardana, M.; Benjamin, C. E.; Li, S.; Shahrivarkevishahi, A.; Popal, S.; Tuong, L. H.; Creswell, C. T.; Gassensmith, J. J. Enhanced Stability and Controlled Delivery of MOF-Encapsulated Vaccines and Their Immunogenic Response In Vivo. *ACS Appl. Mater. Interfaces* **2019**, *11*, 9740−9746.
(32) Zhu, H.; Yin, J.; Wang, X.; Wang, H.; Yang, X. Microorganism-Derived Heteroatom-Doped Carbon Materials for Oxygen Reduction and Supercapacitors. *Adv. Funct. Mater.* **2013**, *23*, 1305−1312.
(33) Amali, A. J.; Sun, J.-K.; Xu, Q. From Assembled Metal−organic Framework Nanoparticles to Hierarchically Porous Carbon for Electrochemical Energy Storage. *Chem. Commun.* **2014**, *50*, 1519−1522.
(34) Chaikittisilp, W.; Hu, M.; Wang, H.; Huang, H.-S.; Fujita, T.; Wu, K. C.-W.; Chen, L.-C.; Yamauchi, Y.; Ariga, K. Nanoporous Carbons Through Direct Carbonization of a Zeolitic Imidazolate Framework for Supercapacitor Electrodes. *Chem. Commun.* **2012**, *48*, 7259−7261.
(35) Salunkhe, R. R.; Kamachi, Y.; Torad, N. L.; Hwang, S. M.; Sun, Z.; Dou, S. X.; Kim, J. H.; Yamauchi, Y. Fabrication of Symmetric Supercapacitors Based on MOF-derived Nanoporous Carbons. *J. Mater. Chem. A* **2014**, *2*, 19848−19854.
(36) Kim, J.; Young, C.; Lee, J.; Heo, Y.-U.; Park, M.-S.; Hossain, M. S. A.; Yamauchi, Y.; Kim, J. H. Nanoarchitecture of MOF-derived Nanoporous Functional Composites for Hybrid Supercapacitors. *J. Mater. Chem. A* **2017**, *5*, 15065−15072.

https://dx.doi.org/10.1021/acsami.9b15667
ACS Appl. Mater. Interfaces XXXX, XXX, XXX−XXX